JOURNAL OF GEOPHYSICAL RESEARCH: OCEANS, VOL. 118, 4334–4345, doi:10.1002/jgrc.20295, 2013

Estimating the Bowen ratio over the open and ice-covered ocean

Edgar L Andreas,[1] Rachel E. Jordan,[2] Larry Mahrt,[3] and Dean Vickers[4]

Received 21 February 2013; revised 28 June 2013; accepted 28 June 2013; published 9 September 2013.

[1] The Bowen ratio, the ratio of the turbulent surface fluxes of sensible (H_s) and latent (H_L) heat, $Bo \equiv H_s/H_L$, occurs throughout micrometeorology. It finds application in the Bowen ratio and energy budget method, where it provides both turbulent heat fluxes when only the available energy at the surface is known. It can yield an estimate of a missing H_s or H_L if the other flux is known. We also suggest that the Bowen ratio may provide the missing piece needed to infer the surface sensible heat flux from satellite data. For this study, we analyze almost 9000 eddy-covariance measurements of H_s and H_L. About half were made over sea ice; the other half, over the open ocean. These are saturated surfaces where the surface specific humidity is the saturation value at the surface temperature. Surface temperatures ranged from −44°C to 32°C and predict the Bowen ratio through the Bowen ratio indicator, $Bo_* = c_p/(L_v \partial Q_{sat}/\partial\Theta)|_{\Theta_s}$. Here c_p is the specific heat of air at constant pressure, L_v is the latent heat of sublimation or vaporization, and $\partial Q_{sat}/\partial\Theta$ is the derivative of the saturation specific humidity (Q_{sat}) with temperature (Θ). All quantities are evaluated at the surface temperature, Θ_s. Although H_s and H_L can occur in nine possible combinations, in our data set, three combinations represent over 90% of the cases: $H_s > 0$ and $H_L > 0$, $H_s < 0$ and $H_L < 0$, and $H_s < 0$ and $H_L > 0$. In each of these three cases, the data suggest $Bo = aBo_*$, where a is 0.40, 3.27, and −0.65, respectively.

Citation: Andreas, E. L, R. E. Jordan, L. Mahrt, and D. Vickers (2013), Estimating the Bowen ratio over the open and ice-covered ocean, *J. Geophys. Res. Oceans*, *118*, 4334–4345, doi:10.1002/jgrc.20295.

1. Introduction

[2] The Bowen ratio,

$$Bo = \frac{H_s}{H_L}, \tag{1}$$

partitions the total turbulent surface heat flux into contributions from sensible heat (H_s) and latent heat (H_L). As a result, the Bowen ratio occurs repeatedly throughout micrometeorology [e.g., *Panofsky and Dutton*, 1984, pp. 92ff., 132, 186; *Garratt*, 1992, pp. 36, 130ff.; *Lewis*, 1995].

[3] A common use for the Bowen ratio is in the *Bowen ratio and energy budget method* [e.g., *Fleagle and Businger*, 1980, p. 290ff.; *Brutsaert*, 1982, p. 210; *Arya*, 1988, p. 191; *Stull*, 1988, p. 274; *Drexler et al*., 2004; *Guo et al*., 2007]. We represent the surface energy budget as

$$0 = Q_{S\downarrow} - Q_{S\uparrow} + Q_{L\downarrow} - Q_{L\uparrow} - G - H_s - H_L. \tag{2}$$

Here Q_S and Q_L are the shortwave and longwave radiative fluxes at the surface, respectively. A down-arrow represents incoming radiation; an up-arrow, outgoing radiation. G is the conductive flux and is positive downward from the surface. In (2), the radiative terms are all taken as positive; H_s and H_L are positive when the flux is from surface to air. Positive terms in (2) thus warm the surface; negative terms cool it.

[4] If we represent the sum of the radiative terms as the net radiation, R_{net} ($= Q_{S\downarrow} - Q_{S\uparrow} + Q_{L\downarrow} - Q_{L\uparrow}$), (1) and (2) let us partition the available energy at the surface, $R_{net} - G$, into sensible and latent heat fluxes:

$$H_s = \frac{Bo(R_{net} - G)}{1 + Bo}, \tag{3a}$$

$$H_L = \frac{R_{net} - G}{1 + Bo}. \tag{3b}$$

That is, this method provides the turbulent fluxes without turbulence measurements.

[5] *Oncley et al*. [2007] and *Foken* [2008], among others, have reported that the energy budget, (2), is often not balanced over land. If this were the general case, (3) would not be useful. In contrast, for our domain, which is sea ice and the open ocean, *Persson et al*. [2002], *Cronin et al*. [2006], and *Persson* [2012], for example, found that the energy budget is balanced within the limits of the experimental uncertainty. Hence, (3) should apply.

[1]NorthWest Research Associates, , Inc. Lebanon New Hampshire, USA.
[2]Jordan Environmental Modeling, PC, Hanover New Hampshire, USA.
[3]NorthWest Research Associates, Inc. Corvallis, Oregon, USA.
[4]College of Earth, Ocean, and Atmospheric Sciences, Oregon State University, Corvallis, Oregon, USA.

Corresponding author: E. L Andreas, NorthWest Research Associates, Inc., 25 Eagle Ridge, Lebanon, NH 03766-1900, USA. (eandreas@nwra.com)

2169-9275/13/10.1002/jgrc.20295

[6] Besides its relevance to the energy budget, other uses of the Bowen ratio are in interpreting sonic anemometer data [*Schotanus et al*., 1983; *Andreas et al*., 1998] and in specifying the Obukhov length, the stratification parameter in the atmospheric surface layer, when the latent heat flux is unknown [e.g., *Busch*, 1973; *Andreas*, 1992]. *Wesley* [1976], *Kunkel and Walters* [1983], *Andreas* [1988], and *Green et al*. [2001] showed how electromagnetic propagation in the surface layer is sensitive to the Bowen ratio.

[7] In bulk flux algorithms (also known as the bulk aerodynamic method), the turbulent surface heat fluxes are usually parameterized as [e.g., *Fairall et al*., 1996, 2003; *Andreas et al*., 2008, 2010a, 2010b]

$$H_s = \rho c_p C_{Hr} S_r (\Theta_s - \Theta_r), \tag{4a}$$

$$H_L = \rho L_v C_{Er} S_r (Q_s - Q_r). \tag{4b}$$

Here ρ is the air density; c_p, the specific heat of air at constant pressure; L_v, the latent heat of vaporization or sublimation; S_r, an effective wind speed at reference height r; Θ_r and Q_r, the potential temperature and specific humidity at r, respectively; and C_{Hr} and C_{Er}, the transfer coefficients for sensible heat and latent heat, respectively, appropriate for height r.

[8] Finally in (4), Θ_s and Q_s are the potential temperature and specific humidity at the surface. In this work, our data come from open and ice-covered oceans. These are *saturated surfaces* such that Q_s is computed as the saturation specific humidity at temperature Θ_s. Other saturated surfaces include large lakes and reservoirs, extensive snow fields, and large glaciers. Our results apply to all such saturated surfaces.

[9] From (4) and (1), we can also represent the Bowen ratio as

$$Bo = \frac{c_p C_{Hr} (\Theta_s - \Theta_r)}{L_v C_{Er} (Q_s - Q_r)}. \tag{5}$$

Thus, if we know the differences $\Theta_s - \Theta_r$ and $Q_s - Q_r$ and have measured either H_s or H_L, we can calculate the other flux by knowing the Bowen ratio (if we also know C_{Hr} and C_{Er} or assume they are equal). Notice also that the signs of $\Theta_s - \Theta_r$ and $Q_s - Q_r$ dictate the signs of H_s, H_L, and Bo.

[10] Over saturated surfaces, the Bowen ratio is constrained. *Philip* [1987] established the theoretical constraint on the Bowen ratio for the case $H_s > 0$ and $H_L > 0$ under the assumption that the near-surface humidity is not above its saturation value, i.e., no fog. *Andreas* [1989; see also *Philip*, 1989] extended Philip's ideas to also formulate constraints for the cases $H_s < 0$, $H_L < 0$ and $H_s < 0$, $H_L > 0$. *Andreas and Cash* [1996] subsequently tested all three of these constraints using data collected over surfaces such as the open ocean, Arctic and Antarctic sea ice, Lake Ontario, marginal seas, and snow-covered ground. *Andreas and Jordan* [2011] continued this type of analysis but used two large data sets collected over sea ice.

[11] Here we add to the *Andreas and Jordan* [2011] data sets a comparably sized data set comprising 13 distinct sets collected over various open ocean regions. In our combined data set, surface temperatures range from −44°C to 32°C and govern the value of the Bowen ratio. For well over 90% of the time in all the individual data sets, the measured sensible and latent heat fluxes collect into one of the three regimes: $H_s > 0$ and $H_L > 0$, $H_s < 0$ and $H_L < 0$, and $H_s < 0$ and $H_L > 0$.

[12] As in *Andreas and Cash* [1996], we define a Bowen ratio indicator function Bo_* that depends approximately exponentially on surface temperature. In each of the three heat flux regimes, $|Bo|$ is similar in magnitude to Bo_* and has the same dependence on surface temperature. Moreover, the data, on average, support the three constraints formulated by *Philip* [1987], *Andreas* [1989], and *Andreas and Cash* [1996]. That is, when $H_s > 0$ and $H_L > 0$, $0 < Bo \le Bo_*$; when $H_s < 0$ and $H_L < 0$, $\infty > Bo \ge Bo_*$; and when $H_s < 0$ and $H_L > 0$, $Bo \approx -Bo_*$. Finally, we make these constraints formal by developing simple, empirical relations that predict Bo from Bo_* in each of the three regimes.

2. Constraints on the Bowen Ratio

[13] Yet another way to formulate the sensible and latent heat fluxes in the atmospheric surface layer is with the turbulent diffusivities for temperature and water vapor, K_θ and K_q, respectively [cf. *Dyer*, 1974; *Philip*, 1987]:

$$H_s = -\rho c_p K_\theta(z) \partial\Theta/\partial z, \tag{6a}$$

$$H_L = -\rho L_v K_q(z) \partial Q/\partial z, \tag{6b}$$

where z is the height. If, as in *Philip* [1987], we assume that K_θ and K_q are equal [e.g., *Högström*, 1996], equations (6) become

$$\frac{H_s}{H_L} = Bo = \frac{c_p \partial\Theta/\partial z}{L_v \partial Q/\partial z} = \frac{c_p}{L_v \partial Q/\partial\Theta}. \tag{7}$$

[14] The right term in (7) comes from the usual assumption that H_s and H_L are constants with height in the atmospheric surface layer over a horizontally homogeneous surface. That is, $(\partial Q/\partial z)/(\partial\Theta/\partial z)$ must also be approximately constant [e.g., *Raupach*, 2001]. Consequently, by chain-rule differentiation, $(\partial Q/\partial z)/(\partial\Theta/\partial z) = \partial Q/\partial\Theta$ is approximately constant.

[15] Without losing generality, we can evaluate $\partial Q/\partial\Theta$ at the surface, which has temperature Θ_s. (In micrometeorology, the physical surface temperature and the potential temperature Θ_s are commonly taken to be the same over surfaces like snow, sea ice, and the open ocean because the potential temperature is referenced to the local surface pressure.) Moreover, for a saturated surface, $Q = Q_{sat}$ when we evaluate $\partial Q/\partial\Theta$ at the surface. Hence, following *Philip* [1987], we define a *Bowen ratio indicator*

$$Bo_* \equiv \left. \frac{c_p}{L_v \partial Q_{sat}/\partial\Theta} \right|_{\Theta_s}. \tag{8}$$

Appendix A gives the equations that we use for evaluating this quantity. Because the saturation vapor pressure used in calculating $\partial Q_{sat}/\partial\Theta$ depends weakly on surface salinity and barometric pressure, Bo_* does too.

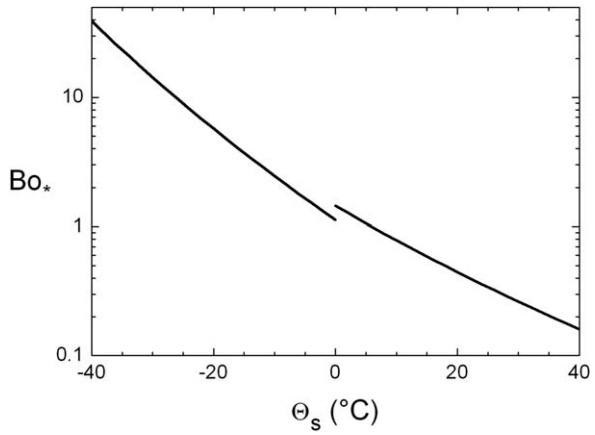

Figure 1. The Bowen ratio indicator Bo_* from (8) as a function of surface temperature Θ_s (see equations in Appendix A). For these calculations, the barometric pressure was 1000 mb and the surface salinity was zero. The discontinuity at $\Theta_s = 0°C$ occurs because the calculation switches from using the saturation vapor pressure over ice and the latent heat of sublimation for L_v for temperatures less than 0°C to using the saturation vapor pressure over water and the latent heat of vaporization for temperatures above 0°C.

[16] Figure 1 shows that Bo_* is a strong function of temperature because the saturation vapor pressure is an exponentially increasing function of temperature. *Philip* [1987], *Andreas* [1989], and *Andreas and Cash* [1996] also showed versions of this plot. Figure 1 corrects minor inconsistencies in the Andreas and Andreas and Cash figures (see Appendix A).

[17] *Priestley and Taylor* [1972] and *Hicks and Hess* [1977] were innovative in using Bo_* to estimate the Bowen ratio and to predict evaporation over saturated surfaces. *Raupach* [2001] formulated a theory of equilibrium evaporation in terms of Bo_*. *Jo et al*. [2002] deduced a climatology for the Bowen ratio over the ocean from Bo_*.

[18] *Philip* [1987] looked exclusively at the case when $H_s > 0$ and $H_L > 0$. Figure 2a is a schematic diagram for this case. The thick, curved line is $Q_{sat}(\Theta)$; above this line is supersaturation, which we assume, following Philip, is a forbidden region (i.e., no fog). At Θ_s, the straight line tangent to the curve is $\partial Q_{sat}/\partial\Theta|_{\Theta_s}$. The shaded area in Figure 2a indicates the region where potential temperature (Θ) and specific humidity (Q) in the air layer near the surface must lie for this flux regime.

[19] From this geometry, we can evaluate $\partial Q/\partial\Theta$ in (7) from

$$\frac{\partial Q}{\partial \Theta} = \lim_{\Delta z \to 0} \frac{\Delta Q}{\Delta \Theta} = \lim_{\Delta z \to 0} \frac{Q_s - Q}{\Theta_s - \Theta}, \tag{9}$$

where Δz is the height increment between the surface and the observations of Θ and Q. Clearly, then

$$\frac{\partial Q}{\partial \Theta} \geq \frac{\partial Q_{sat}}{\partial \Theta}|_{\Theta_s}. \tag{10}$$

Consequently, on combining (7), (8), and (10), we see that

$$Bo \leq Bo_*. \tag{11}$$

[20] *Saunders* [1964, equation (5)] had previously developed a constraint analogous to (10) but replaced $\geq$ with $<$ because his focus was on fog formation.

[21] Besides being positive, both H_s and H_L can conceivably be negative or zero. Thus, there are nine combinations of H_s and H_L. Figure 2 depicts all of these combinations and highlights their implication for constraints on the Bowen ratio. *Andreas* [1989] presented a version of Figure 2 but used water vapor density as the humidity variable because this is the variable that *Philip* [1987] had used. Here we formulate Figure 2 in terms of specific humidity, which is a conservative variable in the atmospheric surface layer.

[22] Some combinations in Figure 2 are forbidden under the assumption of a saturated surface but no supersaturation above the surface: namely, the cases in Figures 2d, 2g, and 2h. The cases $H_s = 0$, $H_L > 0$ (Figure 2b) and $H_s < 0$, $H_L = 0$ (Figure 2f) are trivial because $Bo = 0$ for the former and $Bo = -\infty$ for the latter. In the case $H_s = 0$ and $H_L = 0$ (Figure 2e), Bo is undefined.

[23] Using arguments as above for constraining the $H_s > 0$, $H_L > 0$ case, *Andreas* [1989] showed that the $H_s < 0$, $H_L < 0$ case (Figure 2i) also is constrained by Bo_*. But now the constraint (10) becomes

$$\frac{\partial Q}{\partial \Theta} \leq \left.\frac{\partial Q_{sat}}{\partial \Theta}\right|_{\Theta_s}. \tag{12}$$

As a result, when $H_s < 0$ and $H_L < 0$,

$$Bo \geq Bo_*. \tag{13}$$

[24] Finally, for the case $H_s < 0$, $H_L > 0$, *Andreas and Cash* [1996] hypothesized that, because the line $-\partial Q_{sat}/\partial\Theta|_{\Theta_s}$ cuts through the shaded region in Figure 2c,

$$Bo \approx -Bo_*. \tag{14}$$

[25] Over the saturated surfaces that they studied, *Andreas and Cash* [1996] found that three regimes in Figure 2 dominate: the cases $H_s > 0$, $H_L > 0$; $H_s < 0$, $H_L < 0$; and $H_s < 0$, $H_L > 0$ (Figures 2a, 2i, and 2c, respectively). Over 90% of the measured fluxes that they analyzed fell into one of these combinations.

[26] Figure 3 shows how these three flux regimes may occur over sea ice. Here we used the flux algorithm that *Andreas et al*. [2010b] developed to estimate sensible and latent heat fluxes over winter sea ice. Similar regimes would be found over the ocean although the fluxes would generally have larger magnitudes.

[27] Figure 3 shows fluxes for a wide range in atmospheric stratification, z/L, where L is the Obukhov length and z is the reference height r in (4). In unstable stratification (always without supersaturation above the surface), $H_s > 0$ and $H_L > 0$. In weakly stable stratification, $H_s < 0$ and $H_L > 0$. But in stronger stable stratification, both fluxes are downward: $H_s < 0$ and $H_L < 0$. The flux algorithm predicts no other combinations.

[28] *Andreas and Cash* [1996] found that the constraints (11), (13), and (14) were useful in quantifying the Bowen

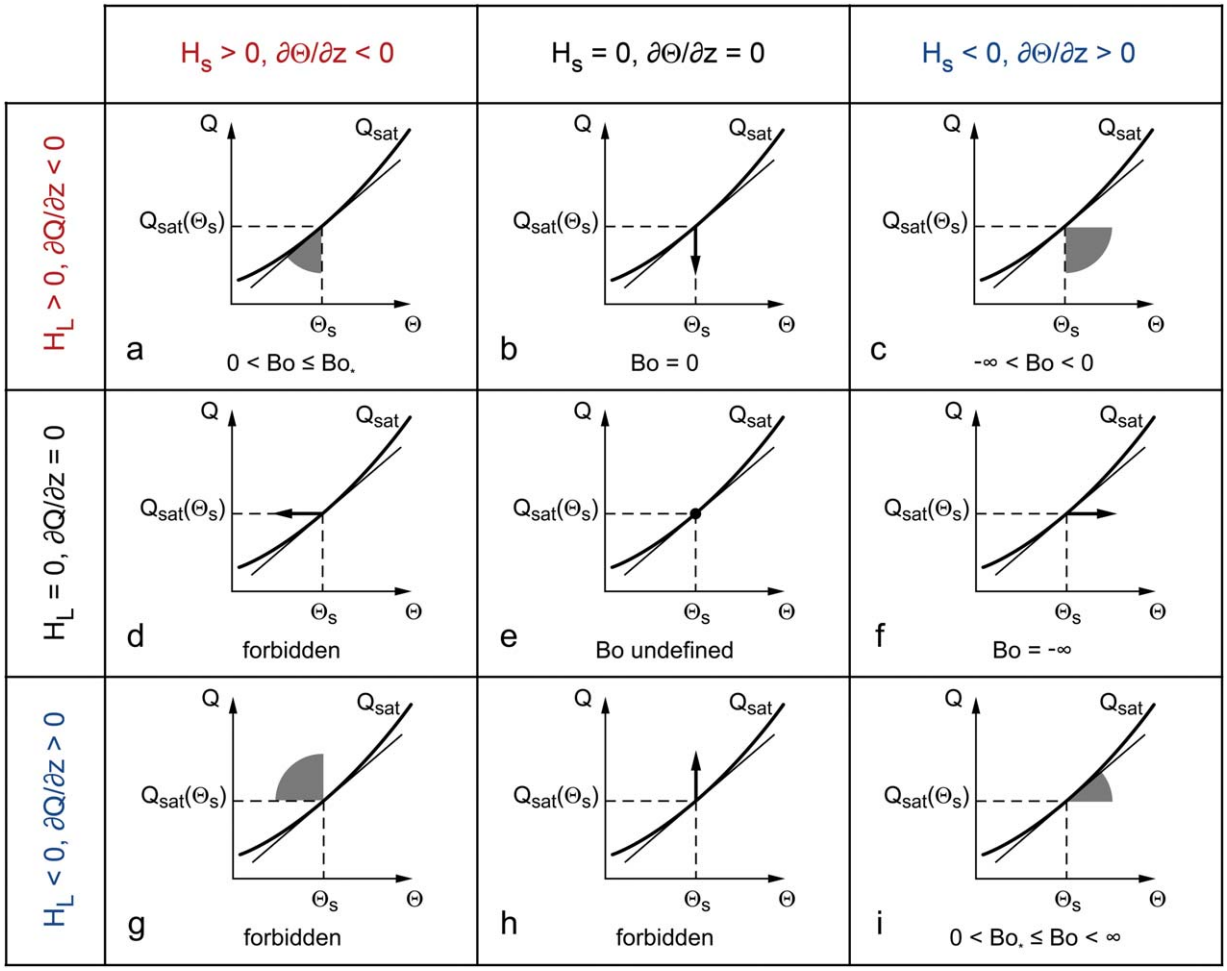

Figure 2. Nine combinations of sensible (H_s) and latent (H_L) heat fluxes and what they say about the Bowen ratio (Bo). The flux is assumed to be down the respective gradient: $\partial\Theta/\partial z$ for sensible heat, and $\partial Q/\partial z$ for latent heat. In each panel, the thicker, curved line is $Q_{sat}(\Theta)$, the relation for saturation in specific humidity as a function of temperature (Θ). Θ_s is the surface temperature; thus, $Q_{sat}(\Theta_s)$ is the specific humidity at the surface. The thin, straight line tangent to the Q_{sat} curve at Θ_s is $\partial Q_{sat}/\partial\Theta|_{\Theta_s}$ and is used in defining Bo_*; see (8). The shaded areas show where the Q and Θ values above the surface must be for the given gradients. Heavy arrows indicate that Q and Θ must lie along these lines. The dot in Figure 2e shows the only possible combination for Q and Θ. Any values of Q and Θ that lie above the $Q_{sat}(\Theta)$ line are forbidden by our assumption that the near-surface humidity is not above saturation.

ratio in these three dominant flux regimes. We repeat some of their analyses here using much larger data sets collected over both sea ice and the open ocean.

3. Data

[29] Table 1 summarizes the data sets that we use in this study. Two large sets were collected over sea ice: one in the Antarctic on Ice Station Weddell; and the second, in the Arctic during SHEBA, the experiment to study the Surface Heat Budget of the Arctic Ocean [*Uttal et al*., 2002]. The other 13 data sets were obtained over the open ocean from a ship, on a platform, and from low-flying aircraft (flight level less than 50 m). The "Reference" column in Table 1 lists citations that provide more information on the data sets.

[30] The "Number of Observations" column in Table 1 shows the number of individual measurements that each data set contributed to our analysis. A useful set of observations had to provide three pieces of information: measurements of Θ_s, H_s, and H_L. A key feature of each data set in Table 1 is that both H_s and H_L were obtained from eddy-covariance measurements. *Mahrt et al*. [2012], *Andreas et al*. [2012], *Vickers et al*. [2013], and the references listed in Table 1 describe the eddy-covariance instruments and the processing; Appendix B summarizes pertinent details.

[31] For the open ocean sets, usually much more data than listed in Table 1 were available; but we screened these data to focus on the measurements most relevant for our analysis.

[32] First, in high winds over the ocean, heat transfer from sea spray droplets augments the interfacial heat fluxes that are parameterized as (4) [*Andreas and DeCosmo*, 2002; *Andreas et al*., 2008; *Andreas*, 2010]. In effect, this spray-mediated heat transfer can sometimes cause a countergradient flux [*Andreas*, 2011] that thereby confuses the

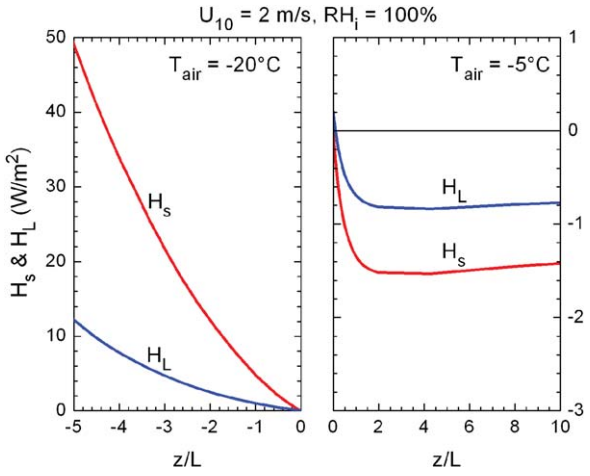

Figure 3. Sensible and latent heat fluxes as a function of surface-layer stratification, z/L (where $z = 10$ m), predicted by the *Andreas et al*. [2010b] winter sea ice flux algorithm. In all cases, the 10 m wind speed (U_{10}) was 2 m s^{-1}, the 10 m relative humidity with respect to ice saturation (RH_i) was 100% [*Andreas et al*., 2002], and the barometric pressure was 1000 mb. In the unstable panel ($z/L < 0$), the 10 m air temperature (T_{air}) was fixed at -20°C, and the surface temperature was incrementally raised from -20°C to produce increasing instability. In the stable panel ($z/L > 0$), the 10 m air temperature was fixed at -5°C, and the surface temperature was lowered from -5°C to produce increasing stability.

definition of the Bowen ratio given by (5). Spray effects, however, appear to be negligible when the 10 m, neutral-stability wind speed, U_{N10}, is less than about 13 m s^{-1} [e.g., *Andreas et al*., 2008]. Hence, from the open ocean data sets, we retain for analysis only data for which $U_{N10} \leq 13$ m s^{-1}. *Andreas et al*. [2012] explain how we calculated U_{N10}.

[33] This screening for wind speed reduced the FASTEX, GFDex, and GOTEX data sets dramatically (by 50% or more) because these experiments sought high winds. The "Number of Observations" for the open ocean sets in Table 1 counts the cases left after this screening.

[34] Second, as explained by *Andreas et al*. [2012], we are concerned that the aircraft flux data in stable stratification may be biased because of vertical flux divergence [e.g., *Wyngaard*, 2010, p. 287] because some flights were at altitudes of 40–50 m. Calculated Bowen ratios then may not represent surface conditions. Therefore, in addition to the screening for wind speed, for our analysis of the Bowen ratio, we further screened the aircraft data for stratification. As in Andreas et al., we retained only the data collected in unstable and weakly stable conditions, $-\infty < z_{ac}/L \leq 0.1$, where z_{ac} is the aircraft flight level and L is the measured Obukhov length. This z_{ac}/L limit for weakly stable stratification is typical of values in the literature; see, for example, *Mahrt et al*. [1998], who suggested 0.06, and *Grachev et al*. [2005], who gave this limit as 0.1.

[35] On the other hand, all of the surface-based observations that we used (Table 1) were made below 20 m. Any vertical flux divergence would be less than the experimental uncertainty for these sets.

4. Flux Regimes

[36] To demonstrate the conceptual utility of Figure 2, we sorted each data set into flux regimes. Table 2 summarizes the results.

[37] In each of the 15 data sets, the three flux regimes $H_s > 0$, $H_L > 0$; $H_s < 0$, $H_L < 0$; and $H_s < 0$, $H_L > 0$ constitute more than 90% of the observed cases. Over the ocean, the $H_s > 0$, $H_L > 0$ regime is dominant by far [cf. *Hsu*, 1998], and the $H_s < 0$, $H_L < 0$ regime is rare.

[38] Over sea ice, the $H_s > 0$, $H_L > 0$ and $H_s < 0$, $H_L < 0$ regimes occur with comparable frequency, although the Ice Station Weddell data may bias this picture. SHEBA was a yearlong deployment, so these data should not be biased by seasonal changes. Ice Station Weddell, however, was only an autumn and early winter experiment.

[39] Table 2 thus confirms what Figure 2 suggests. Of the nine possible combinations for H_s and H_L, several are forbidden by the assumption that the near-surface humidity is not above its saturation value. Other combinations, though permissible, are meteorologically rare: namely, cases when either H_s or H_L is measured to be exactly zero. Random variability in the turbulence measurements that can cause the measured flux to have the wrong sign, especially when the fluxes have small magnitudes, in part explains why the three flux regimes do not always total 100% of the cases. This variability, in particular, explains why the "Total" entries for the SHEBA and Ice Station Weddell sets in Table 2 are smaller than all but the Monterey entry for the over-ocean sets. Over sea ice, both the sensible and latent heat fluxes are generally small.

5. *Bo-Bo*$_*$ Relations

[40] Figures 4–6 show Bo versus Bo_* for all the data sets summarized in Table 1. From the sea ice and ocean data sets, we have over 4700 observations in the $H_s > 0$, $H_L > 0$ regime (Figure 4), almost 1500 observations in the $H_s < 0$, $H_L < 0$ regime (Figure 5), and over 1300 observations in the $H_s < 0$, $H_L > 0$ regime (Figure 6). The only comparable previous analysis was by *Andreas and Cash* [1996], but they had only about 1200 observations total.

[41] The data points in Figures 4–6 are quite scattered. One reason is that the usual uncertainty in eddy-covariance measurements of sensible and latent heat flux is $\pm 20\%$ for each flux [e.g., *Fairall et al*., 1996; *Finkelstein and Sims*, 2001; *Persson et al*., 2002; *Andreas et al*., 2010b]. Thus, the typical uncertainty in any individual measurement of the Bowen ratio is $\pm 40\%$. But when either flux is small—which they almost always are over sea ice [*Persson et al*., 2002; *Andreas et al*., 2004, 2010a, 2010b]—uncertainties in individual values can approach $\pm 100\%$.

[42] Therefore, one lesson from Figures 4–6 is that you need a lot of data to overcome the inherent random errors and thus to see the average tendencies in the phenomenon. Hence, besides individual values, Figures 4–6 show geometric mean Bowen ratios within bins of Bo_*. We base bin averages on the geometric mean because the Bowen ratios in a bin have an approximately lognormal distribution. Each such plotted average also has ± 2 standard deviation error bars. These error bars thus delimit 95% confidence limits for the Bowen ratio population within each bin. Bin medians, also shown in these plots, agree well with the

Table 1. The Data Sets Used in This Study[a]

Data Set	Number of Observations	Platform/Location	Reference
Ice Station Weddell	1031	Tower on sea ice, western Weddell Sea	*Andreas et al*. [2004, 2005]
SHEBA	2859	Tower on sea ice, Beaufort Gyre, Arctic Ocean	*Persson et al*. [2002], *Andreas et al*. [2010a, 2010b]
FASTEX	136	*R/V Knorr*, transect across the North Atlantic	*Persson et al*. [2005]
GFDex	11	FAAM BAE 146 aircraft, Irminger Sea and Denmark Strait	*Petersen and Renfrew* [2009]
HEXOS	109	Meetpost Noordwijk platform, North Sea	*DeCosmo* [1991], *DeCosmo et al*. [1996]
CARMA4	627	CIRPAS Twin Otter, off coast of southern California	*Vickers et al*. [2013]
CBLAST-weak	760	Long-EZ aircraft, Martha's Vineyard, Massachusetts	*Edson et al*. [2007]
GOTEX	341	NCAR C-130, Gulf of Tehuantepec	*Romero and Melville* [2010]
MABLEB	29	CIRPAS Twin Otter, off Monterey, California	*Vickers et al*. [2013]
Monterey	453	CIRPAS Twin Otter, off Monterey, California	*Mahrt and Khelif* [2010]
POST	189	CIRPAS Twin Otter, off Monterey, California	*Vickers et al*. [2013]
RED	366	CIRPAS Twin Otter, east of Oahu, Hawaii	*Anderson et al*. [2004]
SHOWEX Nov '97	508	Long-EZ aircraft, off coast of Virginia and North Carolina	*Sun et al*. [2001]
SHOWEX Nov '99	794	Long-EZ aircraft, off coast of Virginia and North Carolina	*Sun et al*. [2001]
TOGA COARE	760	NCAR Electra, western equatorial Pacific Ocean	*Sun et al*. [1996], *Vickers and Esbensen* [1998]

[a]The first two sets are the sea ice sites; the remaining data sets were collected over the open ocean. The "Number of Observations" is the number of cases used to analyze the H_s and H_L regimes (Table 2). Because of the second screening of the aircraft data for stratification (i.e., for $z_{ac}/L \leq 0.1$), fewer cases are used in the *Bo*-*Bo*$_*$ analyses (Figures 4–6). The "Reference" provides additional details on a data set. *Mahrt et al*. [2012], *Andreas et al*. [2012], and *Vickers et al*. [2013] also provide more information on the open ocean sets. SHEBA is the Surface Heat Budget of the Arctic Ocean experiment. FASTEX is the Fronts and Atlantic Storm-Tracks Experiment. GFDex is the Greenland Flow Distortion experiment. HEXOS is Humidity Exchange over the Sea. CARMA4 is the Cloud-Aerosol Research in the Marine Atmosphere experiment, 4. CBLAST is the Coupled Boundary Layers and Air-Sea Transfer experiment. GOTEX is the Gulf of Tehuantepec Experiment. MABLEB is the Marine Atmospheric Boundary Layer Energy Budget experiment. POST is the Physics of the Stratocumulus Top experiment. RED is the Rough Evaporation Duct experiment. SHOWEX is the Shoaling Waves Experiment. TOGA COARE is the Tropical Ocean-Global Atmosphere Coupled Ocean-Atmosphere Response Experiment.

Table 2. Dominant Heat Flux Regimes[a]

Data Set	$H_s > 0$ $H_L > 0$ (%)	$H_s < 0$ $H_L < 0$ (%)	$H_s < 0$ $H_L > 0$ (%)	Total, These Three Cases (%)
Ice Station Weddell	31.6	43.6	15.3	90.5
SHEBA	36.4	31.0	25.8	93.2
FASTEX	86.8	1.5	10.3	98.6
GFDex	100.0	0.0	0.0	100.0
HEXOS	89.9	0.0	10.1	100.0
CARMA4	61.6	13.7	19.8	95.1
CBLAST-weak	46.7	33.4	15.1	95.2
GOTEX	63.3	0.0	36.1	99.4
MABLEB	69.0	0.0	31.0	100.0
Monterey	82.6	0.4	8.8	91.8
POST	73.5	9.5	12.2	95.2
RED	97.8	0.0	2.2	100.0
SHOWEX Nov '97	65.8	0.0	34.2	100.0
SHOWEX Nov '99	71.7	12.7	12.3	96.7
TOGA COARE	94.5	0.4	3.9	98.8

[a]The three H_s and H_L columns list the percentage of the total cases in each H_s and H_L flux regime. The last column is the percentage of total cases that occurred in these three regimes.

averages and therefore imply that the $\ln(|Bo|)$ values within a bin are symmetrically distributed about the geometric mean, as they would be in a lognormal distribution.

[43] Figures 4–6 all show a gap in the data near $Bo_* = 1$. Figure 1 helps explain this gap. Over sea ice, which by definition must have a surface temperature of 0°C or lower, Bo_* has a minimum value of 1.12. Meanwhile, over the open ocean (assumed salinity of 34 psu), Bo_* will be near 1 when the surface temperature is 5.9°C–6.5°C. The GFDex set does have temperatures in this range, but we eliminated these cases when we screened out U_{N10} values above 13 m s^{-1}. The surviving GFDex cases have surface temperatures near 0°C, and those points appear as the few red points among the blue points where Bo_* is between 1 and 2 in Figures 4–6.

[44] Because Figures 4–6 are log-log plots, a first option would be to represent the Bowen ratio as

$$Bo = aBo_*^b. \tag{15}$$

Determining a and b from least squares linear regression would then require fitting

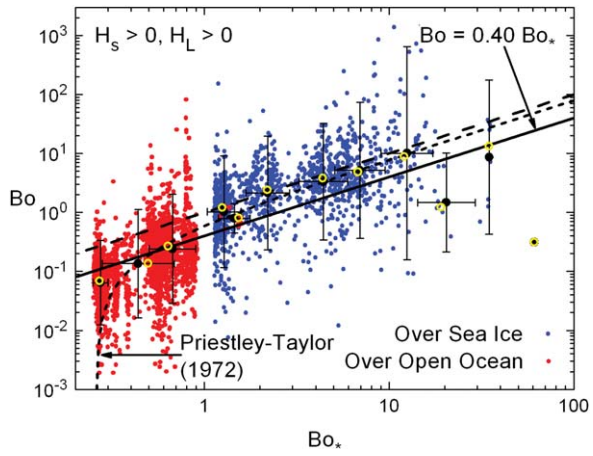

Figure 4. The Bowen ratio is calculated from the measured values of H_s and H_L in the data sets in Table 1 and compared with corresponding values of Bo_* computed from (8) (using the algorithm in Appendix A). The plot is for the case when $H_s > 0$ and $H_L > 0$. The correlation coefficient for the points in this log-log plot is 0.780. The two colors distinguish data collected over sea ice and over the open ocean. The bigger black circles are averages (computed as the geometric mean) in Bo_* bins, where there are four bins per decade. The error bars are ± 2 standard deviations and thus represent 95% confidence intervals for the bin populations. The yellow circles denote medians of both Bo and Bo_* in the Bo_* bins. The Bo_* range between 1 and 2 has two averages and two medians: one each for the ocean cases and for the sea ice cases. The black dashed line is 1:1; the solid black line is (17); the line with shorter dashes is *Priestley and Taylor*'s [1972] equation, (21).

$$\ln(|Bo|) = \ln(|a|) + b\ln(Bo_*). \tag{16}$$

(The absolute values are invoked only for the $H_s < 0$, $H_L > 0$ case.)

[45] In each of Figures 4–6, however, both the bin averages and the bin medians suggest a slope that tends to parallel the 1:1 line. That is, b would be 1 in (16), and $|Bo| \propto Bo_*$ from (15). Hence, in each of Figures 4–6, the solid line shows the best fit through the data with b fixed at 1 in (16).

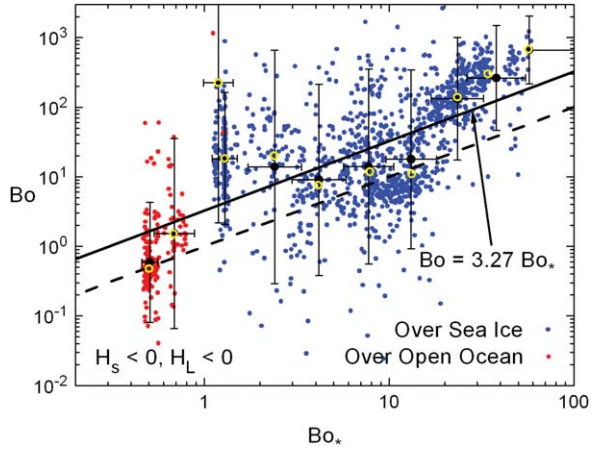

Figure 5. As in Figure 4, but this shows the cases for which $H_s < 0$ and $H_L < 0$. The solid black line is (18), and the correlation coefficient is 0.655.

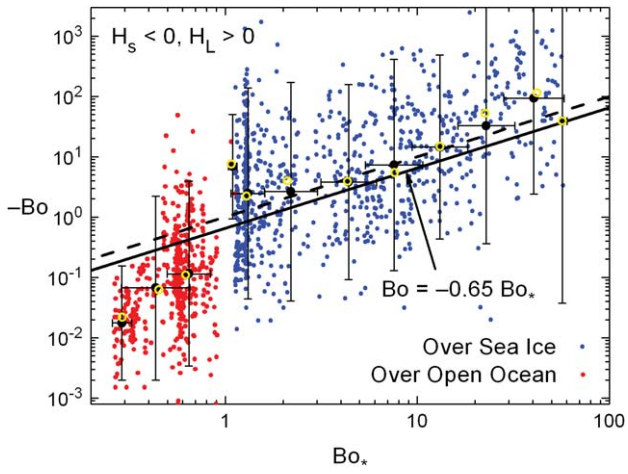

Figure 6. As in Figure 4, but this shows the cases for which $H_s < 0$ and $H_L > 0$. The solid black line is (19), and the correlation coefficient is 0.709.

[46] For the $H_s > 0$, $H_L > 0$ plot (Figure 4), we obtain

$$Bo = (0.40 \pm 0.02)Bo_*; \tag{17}$$

for the $H_s < 0$, $H_L < 0$ plot (Figure 5),

$$\mathrm{Bo} = (3.27 \pm 0.30)Bo_*; \tag{18}$$

and for the $H_s < 0$, $H_L > 0$ plot (Figure 6),

$$Bo = -(0.65 \pm 0.08)Bo_*. \tag{19}$$

[47] The uncertainties in (17)–(19) are computed from the standard deviations in the geometric means of all of the Bo and Bo_* values in each regime. In effect, these uncertainties are approximately ± 2 standard deviations for the associated coefficient and thus give its 95% confidence interval.

[48] Equation (17) has nearly the same coefficient that *Andreas and Cash* [1996] obtained for the $H_s > 0$, $H_L > 0$ case, 0.38. Thus, we again confirm *Philip*'s [1987] original theoretical result that, on average, $Bo \leq Bo_*$ when $H_s > 0$ and $H_L > 0$, the surface is saturated, but the near-surface humidity is not above its saturation value.

[49] The coefficient in (18) is about three times larger than in *Andreas and Cash*'s [1996] analysis. But they had fewer than 170 observations in this $H_s < 0$, $H_L < 0$ regime and only 15 observations collected over the open ocean. Equation (18) is thus a more accurate result. Nevertheless, as with Andreas and Cash's analysis, this regime produces the coefficient with the largest uncertainty. Still, our new result and Andreas and Cash's confirm *Andreas*'s [1989] conclusion that $Bo \geq Bo_*$, on average, when $H_s < 0$ and $H_L < 0$.

[50] Our (19) is similar to *Andreas and Cash*'s [1996] result for the $H_s < 0$, $H_L > 0$ regime: Our coefficient is -0.65; theirs is -0.32. Consequently, we, too, support the suggestion by Andreas and Cash that $Bo \approx -Bo_*$ in the $H_s < 0$ and $H_L > 0$ regime.

[51] In summary, our analyses—represented in Figures 4–6 and in (17)–(19)—suggest the general tendency that over saturated surfaces, $|Bo|$ always increases proportionately to Bo_*.

6. Discussion

6.1. The Historical Linear Relations

[52] *Priestley and Taylor* [1972] and *Hicks and Hess* [1977] did seminal work on predicting the Bowen ratio over saturated surfaces. The Priestley-Taylor method, especially, is still used frequently [e.g., *Eichinger et al*., 1996; *Kim and Entekhabi*, 1997; *Drexler et al*., 2004; *Guo et al*., 2007]. Both Priestley and Taylor and Hicks and Hess predicted *Bo* from a linear function of Bo_* but only over water surfaces and only for the $H_s > 0$ and $H_L > 0$ regime.

[53] *Priestley and Taylor* [1972] deduced a single empirical coefficient α. In our terminology, their result is

$$Bo = \frac{1}{\alpha} Bo_* - \left(1 - \frac{1}{\alpha}\right), \tag{20}$$

where $\alpha = 1.26$. That is, (20) becomes

$$Bo = 0.794\, Bo_* - 0.206 \tag{21}$$

for the $H_s > 0$, $H_L > 0$ case. Figure 4 shows (21).

[54] *Hicks and Hess* [1977] fitted two coefficients, the slope and the intercept of the linear relation. Their result is

$$Bo = 0.63\, Bo_* - 0.15. \tag{22}$$

[55] Both (21) and (22) thus support *Philip*'s [1987] suggestion that $Bo \leq Bo_*$ when $H_s > 0$ and $H_L > 0$. But both also predict negative Bowen ratios in the $H_s > 0$, $H_L > 0$ regime if the water temperature is high enough. Equation (21) gives negative *Bo* if $Bo_* < 0.256$; (22), if $Bo_* < 0.24$. For freshwater, Figure 1 (or the equations in Appendix A) associates a surface temperature of 30.6°C with $Bo_* = 0.256$ and 31.8°C with $Bo_* = 0.24$. For saline ocean water, each temperature would be about 0.3°C higher. In other words, at water temperatures attainable over the tropical ocean, both (21) and (22) would predict a negative Bowen ratio for an analysis that presumes a positive Bowen ratio. Figure 4 emphasizes this shortcoming by showing how (21) falls rapidly below the data for $Bo_* < 0.3$, where surface temperatures are above 28°C.

[56] Moreover, neither *Priestley and Taylor* [1972] nor *Hicks and Hess* [1977] had data for which the surface temperature was less than 10°C. Hence, they did not treat Bo_* values greater than about 0.8. Figures 4–6 show that over open water Bo_* can exceed this value; and over sea ice, Bo_* can greatly exceed this value. But Figure 4 surprisingly also shows that the Priestley-Taylor result (21) is a reasonable approximation over sea ice because, in effect, it becomes $Bo = 0.794\, Bo_*$ for large Bo_*, which is close to our (17).

[57] The limited range of conditions that *Priestley and Taylor* [1972] and *Hicks and Hess* [1977] explored explain why they could fit *Bo*-versus-Bo_* data with linear relations. *Guo et al*. [2007] likewise recently evaluated the Priestley-Taylor α over a limited temperature range, 20°C–31°C, for the $H_s > 0$ and $H_L > 0$ regime and found α to be in the range 1.1–1.3. But when Guo et al. attempted to evaluate α in the $H_s < 0$, $H_L < 0$ and $H_s < 0$, $H_L > 0$ regimes, they found it to be much more variable.

[58] For these several reasons, we believe that our exponential relations between *Bo* and Bo_* (with the exponent equal one; (17)–(19)), provide a more unifying approach to predicting the Bowen ratio than do linear relations.

6.2. Equilibrium Evaporation

[59] *Raupach* [2001] explained the condition for *equilibrium evaporation* ($H_{L,eq}$). In our notation, his condition is [see also *De Bruin and Keijman*, 1979; *Lhomme*, 1997]

$$\frac{1}{1 + Bo_*} = \frac{H_{L,eq}}{H_s + H_{L,eq}} = \frac{H_{L,eq}}{R_{net} - G}. \tag{23}$$

The denominators of both the middle and right terms are usually called the available energy (see (2)). *McNaughton* [1976] preferred to call the $H_{L,eq}$ given by (23) the *quasi-equilibrium evaporation*.

[60] Because these papers are treatises on "evaporation," $H_{L,eq}$ is explicitly positive. The available energy is also assumed to be positive. Hence, (23) applies only for the $H_s > 0$, $H_L > 0$ flux regime.

[61] On using the Bowen ratio to simplify the middle term in (23), we obtain

$$\frac{1}{1 + Bo_*} = \frac{1}{1 + Bo_{eq}}, \tag{24}$$

where Bo_{eq} is the Bowen ratio formed from the equilibrium evaporation. As a result,

$$Bo_{eq} = Bo_* \tag{25}$$

[62] In other words, most theoretical studies of equilibrium evaporation produce predictions that align with our experimental results. But unlike these theoretical results, which treat only the $H_s > 0$, $H_L > 0$ regime, our experimental results suggest the approximate relation

$$|Bo| \approx Bo_* \tag{26}$$

for each of the three dominant flux regimes (see (17)–(19)).

6.3. Appropriate Spatial and Temporal Scales

[63] The scatter in Figures 4–6 is obvious and pertinent. As we explained earlier, some of this scatter results from random measurement errors. But as important is a clear interpretation of what Figure 2 implies about the possibility of unique *Bo*-Bo_* relations. For the three regimes that we consider—Figures 2a, 2c, and 2i—theory tells us only that the temperature and specific humidity of the near-surface air must fall somewhere in the shaded areas. That is, for any given Bo_*, a host of Bowen ratios is possible.

[64] This interpretation is also in line with Monin-Obukhov similarity theory. Over a saturated surface with a given surface temperature (and, thus, a given surface specific humidity), a wide variety of air temperatures and specific humidities yield convergent solutions for the similarity equations [e.g., *Andreas et al*., 2008, 2010a, 2010b].

[65] As a consequence, individual estimates of the Bowen ratio from any of (17)–(19) will rarely agree perfectly with individual measurements of *Bo*—from eddy-covariance instruments, for instance. Only with averaging did the scattered points in Figures 4–6 reveal any consistent relationship between *Bo* and Bo_*. We therefore interpret (17)–(19) to represent only average behavior of the heat fluxes over saturated surfaces.

[66] Following the conclusions in *Priestley and Taylor* [1972] and *Hicks and Hess* [1977], *Andreas and Cash* [1996] acknowledged that (17)–(19) are most appropriate if they are applied to data that have been time-averaged or represent average conditions over a large horizontal area. We here reiterate that (17)–(19) and our distributions summarized in Table 2 will be most useful when they are applied to data that are, in some sense, averaged. A spatial average could be over a grid cell in a large-scale atmospheric model, over a satellite footprint, or along a surface-layer scintillometer's averaging path.

[67] An appropriate temporal average for point measurements is on the order of a day [e.g., *De Bruin and Keijman*, 1979]. If the flux regime—represented as in (17)–(19)—changes during this averaging period, even this temporal averaging may produce ambiguous results. On a positive note, though, flux regimes over the open and ice-covered ocean are usually long lasting.

6.4. Fluxes From Satellites

[68] Obtaining surface heat fluxes from satellites is one of the objectives that motivates this study and is also a natural application implied in the preceding subsection. Current methods for obtaining surface fluxes from satellites are always based on a bulk flux algorithm, such as represented by (4) [e.g., *Liu*, 1988; *Thadathil et al*., 1995; *Konda et al*., 1996]. Consequently, from satellites, we need surface temperature and surface-level estimates of wind speed, air temperature, and humidity.

[69] Over water, scatterometers or synthetic aperture radar can provide wind speed. Advanced very high resolution radiometers (AVHRR) can provide surface temperature, Θ_s, and thus surface humidity, Q_s.

[70] The necessary near-surface gradients $\Theta_s - \Theta_r$ and $Q_s - Q_r$ are typically found by first estimating the total precipitable water from the scanning multichannel microwave radiometer [*Liu*, 1988] or the Special Sensor Microwave/Imager [*Thadathil et al*., 1995; *Bentamy et al*., 2003]. The next step, often, is to obtain surface-level humidity, Q_r, from a relation between precipitable water and Q_r such as those described by *Liu* [1986] or *Schulz et al*. [1993] [e.g., *Liu*, 1988; *Konda et al*., 1996; *Bentamy et al*., 2003]. This is sufficient information to make a crude estimate of the latent heat flux from (4b).

[71] We say "crude" because estimating the sensible heat flux and thus correcting C_{Er} in (4b) for stratification effects [see *Andreas et al*., 2008, 2010a, 2010b; *Fairall et al*., 1996, 2003] have been troublesome because no satellite measurements have been found for the near-surface air temperature Θ_r or for the temperature gradient $\Theta_s - \Theta_r$. Often, the sensible heat flux is thus ignored for open ocean applications. *Thadathil et al*. [1995], however, developed a statistical relation between in situ measurements of Θ_r and the satellite-derived estimate of Q_r from precipitable water. *Jackson and Wick* [2010] similarly developed a statistical relation that correlates in situ measurements of Θ_r with three satellite variables: AVHRR measurements of Θ_s and Advanced Microwave Sounder Unit A brightness temperatures at 52.8 and 53.6 GHz.

[72] Our analysis here, however, suggests a simpler approach. From the AVHRR measurement of Θ_s, we can calculate Bo_* and thus estimate *Bo* from (17) to (19). Because the standard satellite techniques provide a first estimate of H_L, H_s now comes easily from the satellite estimate of *Bo*. Iteratively solving (4) and the equations for the momentum flux and the Obukhov length using these values of H_s and H_L provides improved estimates of the transfer coefficient C_{Er} and, in turn, increasingly better estimates of H_L and H_s.

[73] Alternatively, if satellite observations could provide the net surface radiation, R_{net}, both sensible and latent heat fluxes could be obtained from (3) and an estimate of the Bowen ratio derived from (17)–(19).

7. Conclusions

[74] With almost 9000 eddy-covariance observations over both sea ice and the open ocean, where surface temperatures ranged from -44°C to 32°C, this is, to our knowledge, the most encompassing survey to date of the Bowen ratio over saturated surfaces.

[75] Though nine combinations of H_s and H_L are conceivable—both H_s and H_L can be positive, negative, or zero—three combinations dominate our data: $H_s > 0$, $H_L > 0$; $H_s < 0$, $H_L < 0$; and $H_s < 0$, $H_L > 0$. In the sea ice data sets, these three combinations constitute over 90% of the observations. In 12 of the 13 open ocean data sets, they represent at least 95% of the observations. For the one exception (Monterey, Table 2), they still represent 91.8% of the observations.

[76] Furthermore, in these three regimes, the average behavior of the resulting Bowen ratio ($\equiv H_s/H_L$) is constrained by the Bowen ratio indicator Bo_* (see (8)). For the $H_s > 0$, $H_L > 0$ regime, we confirm *Philip*'s [1987] postulated constraint: $Bo \le Bo_*$. For the $H_s < 0$, $H_L < 0$ regime, we likewise confirm *Andreas*'s [1989] conclusion: $Bo \ge Bo_*$. Finally, our data in the $H_s < 0$, $H_L > 0$ regime support *Andreas and Cash*'s [1996] suggestion that $Bo \approx -Bo_*$. Equations (17)–(19) represent these results.

[77] These conclusions come with one caveat. Over the ocean in 10 m winds, nominally, above 13 m s^{-1}, heat transfer mediated by sea spray can significantly influence the fluxes of latent and sensible heat. Because these spray-mediated fluxes do not scale the same way the interfacial fluxes do—that is, as in (4) or (6)—the Bowen ratio is no longer unambiguously related to the temperature and humidity gradients (see (5) and (7)). Therefore, from our analysis, we excluded data in the ocean sets that were collected when $U_{N10} > 13$ m s^{-1}; our conclusions, thus, do not necessarily apply over the open ocean when winds are above 13 m s^{-1}.

[78] We envision several possible uses for our results. One is as a quality control on measurements or model estimates of H_s and H_L. The values obtained should have a climatology similar to those in Table 2. The inferred Bowen ratio should also depend on surface temperature as predicted in (17)–(19). In fact, (17)–(19) can provide an estimate of the Bowen ratio in any of the many applications

Table 3. Quantities From *Buck* [1981] That We Use in (A6)[a]

	Saturation Over Ice ($\Theta < 0°C$)	Saturation Over Water ($\Theta \geq 0°C$)
e_0 (mb)	6.1115	6.1121
$P_0(P)$	$1.0003 + 4.18 \times 10^{-6}P$	$1.0007 + 3.46 \times 10^{-6}P$
A	22.452	17.502
B (°C)	272.55	240.97

[a]See also *Andreas* [2005]. In the second row, P is in mb.

that require it as long as the data represent adequate temporal or spatial averaging.

[79] In particular, (17)–(19) provide partitioning of the sensible and latent heat fluxes and thus could be key components for estimating the surface energy budget from satellite data over saturated surfaces like the ocean, large lakes, sea ice, snow-covered tundra, or the Greenland or Antarctic ice sheets.

Appendix A: Calculating Bo_*

[80] *Andreas and Cash* [1996] give equations for calculating Bo_* from (8). Because their derivation has some minor inconsistencies, however, we rederive the equations here.

[81] For obtaining c_p and L_v, we use the functions summarized by *Andreas* [2005]. For c_p, the specific heat of air at constant pressure,

$$c_p = 1005.60 + 0.017211\Theta + 0.000392\Theta^2, \qquad \text{(A1)}$$

where c_p is in J kg^{-1} °C^{-1} and Θ is the temperature in °C. For the latent heat of vaporization (L_v) or sublimation (L_s),

$$L_v = (25.00 - 0.02274\ \Theta) \times 10^5 \qquad \text{for } \Theta \geq 0^\circ\text{C} \qquad \text{(A2)}$$

and

$$L_s = (28.34 - 0.00149\Theta) \times 10^5 \qquad \text{for } \Theta < 0^\circ\text{C} \qquad \text{(A3)}$$

In (A2) and (A3), L_v and L_s are in J kg^{-1}, and Θ is again the temperature in °C.

[82] From the ideal gas law for dry air and water vapor, the specific humidity (Q) can be written as [e.g., *Andreas*, 2005]

$$Q = \frac{0.622(e/P)}{1 - 0.378(e/P)}, \qquad \text{(A4)}$$

where e is the vapor pressure and P is the barometric pressure. Here the constants are $0.622 = M_w/M_a$ and $0.378 = 1 - M_w/M_a$, where M_w ($= 18.015 \times 10^{-3}$kg mol^{-1}) is the molecular weight of water and M_a ($= 28.9644 \times 10^{-3}$kg mol^{-1}) is the molecular weight of dry air. The required derivative in (8) thus becomes

$$\frac{\partial Q_{sat}}{\partial \Theta} = \frac{Q_{sat}}{\{1 - 0.378(e_{sat}/P)\}e_{sat}} \frac{\partial e_{sat}}{\partial \Theta}, \qquad \text{(A5)}$$

where subscript *sat* denotes the values for saturation.

[83] For the saturation vapor pressure, e_{sat}, we use the equations from *Buck* [1981]. For saturation over both ice and water, these equations have the general form

$$e_{sat}(\Theta, P) = e_0 P_0(P) \exp\left(\frac{A\Theta}{B + \Theta}\right), \qquad \text{(A6)}$$

where e_0, A, and B are constants and P_0 is a function of pressure P. The required derivative in (A5) is thus simply

$$\frac{\partial e_{sat}}{\partial \Theta} = \left\{\frac{AB}{(B + \Theta)^2}\right\} e_{sat}(\Theta, P). \qquad \text{(A7)}$$

Table 3 lists the constants e_0, A, and B and the function $P_0(P)$.

[84] On substituting (A5) and (A7) into (8), we obtain a programmable function for Bo_*:

$$Bo_* = \frac{c_p(\Theta_s)[1 - 0.378\{e_{sat}(\Theta_s, P, S)/P\}]}{L_v(\Theta_s) Q_{sat}(\Theta_s, P, S)} \left\{\frac{(B + \Theta_s)^2}{AB}\right\}. \qquad \text{(A8)}$$

[85] Notice, e_{sat} and Q_{sat} both depend on salinity, S. In obtaining e_{sat} from (A6) and Q_{sat} from (A4), we must account for the depression in the saturation vapor pressure if the surface is saline. That is,

$$e_{sat}(\Theta_s, P, S) = e_{sat}(\Theta_s, P) f(S), \qquad \text{(A9)}$$

where $e_{sat}(\Theta_s,P)$ comes from (A6) and

$$f(S) = 1 - 0.000537S, \qquad \text{(A10)}$$

where S is the salinity in psu.

Appendix B: Measurement Details

[86] For completeness, we briefly discuss the instruments and processing used to obtain the sensible and latent heat fluxes in our data set. The SHEBA, FASTEX, and Ice Station Weddell experiments (Table 1) used similar instruments. All three measured the three turbulent velocity components and the turbulent fluctuations in temperature with sonic anemometer/thermometers. Ice Station Weddell used a Lyman-α hygrometer to measure the turbulent humidity fluctuations; SHEBA and FASTEX used an Ophir hygrometer.

[87] The temperature that a sonic anemometer/thermometer measures is the so-called *sonic temperature*, which has a slight contribution from humidity [*Schotanus et al.*, 1983; *Kaimal and Gaynor*, 1991]. In the FASTEX data set, sensible heat fluxes were corrected for this humidity contribution [*Persson et al.*, 2005]. *Grachev et al.* [2005] explained that, in the SHEBA data set, this moisture correction was negligible because of the very small latent heat fluxes. *Andreas et al.* [1998] likewise showed that this moisture correction is negligible when the Bowen ratio is large, which translates to $|Bo|$ greater than roughly 0.5 for the sea ice sets. Hence, there is no humidity correction in the Ice Station Weddell sensible heat fluxes [*Andreas et al.*, 2005], but the SHEBA sensible heat fluxes do include this

minor humidity correction [*Persson et al*., 2002; *Grachev et al*., 2005].

[88] All of the aircraft listed in Table 1 used pressure sensors to measure the turbulent velocity components [*Andreas et al*., 2012] and platinum resistance thermometers or bead thermistors to measure the turbulent temperature fluctuations. Therefore, no extra corrections are necessary for the sensible heat fluxes in these data sets.

[89] As with FASTEX, SHEBA, and Ice Station Weddell, all of the aircraft in Table 1 measured the turbulent humidity fluctuations with optical absorption sensors: namely, Lyman-α, krypton, or ultraviolet hygrometers. Because all such sensors yield water vapor density as the fundamental measurement, the so-called *Webb correction* [*Webb et al*., 1980; *Fairall et al*., 1996; *Fuehrer and Friehe*, 2002] can be necessary if these densities are used directly for computing the latent heat flux. Such corrections were made to the latent heat fluxes in the SHEBA, FASTEX, and Ice Station Weddell data sets. It is unclear from *Petersen and Renfrew* [2009] whether they made the Webb correction in their GFDex set, but we used only 11 observations from this set.

[90] We processed the aircraft sets in Table 1 from CARMA4 to TOGA COARE ourselves. For these, we obviated the Webb correction by converting the raw water vapor densities to specific humidities before any flux calculations.

[91] The HEXOS experiment used propeller anemometers to measure the turbulent velocity vector and thermocouples to measure the temperature fluctuations. Thus, no corrections to sensible heat flux were necessary. The turbulent humidity fluctuations were measured with both a Lyman-α hygrometer and wet and dry thermocouples. In our analysis, when latent heat fluxes from both the Lyman-α and wet and dry thermocouples were available for a HEXOS run, we used the average of the two for H_L.

[92] It is not clear whether *DeCosmo et al*. [1996] or *DeCosmo* [1991] applied the Webb correction to their latent heat flux data. If they did not, we estimate that absolute values of errors in the reported latent hear fluxes would be at most 4 W m^{-2} and would usually be much less. Because all tabulated latent heat fluxes in the HEXOS set are larger than 4 W m^{-2}, a missing Webb correction would not change the results in Table 2 and would have negligible effects on Figures 4 and 6.

[93] **Acknowledgments.** We thank our colleagues in the Atmospheric Surface Flux Group for helping us collect, process, and interpret the SHEBA data: Chris Fairall, Andrey Grachev, Peter Guest, Tom Horst, and Ola Persson. We thank the other members of the meteorological team on Ice Station Weddell for their help: Kerry Claffey, Boris Ivanov, and Aleksandr Makshtas. We thank the following colleagues for providing the open ocean data sets: Ola Persson, Jeff Hare, Chris Fairall, and Bill Otto for the FASTEX set; Nína Petersen and Ian Renfrew for the GFDex set; and Janice DeCosmo for help with the HEXOS set. We thank Emily Moynihan for preparing Figure 2. We deeply appreciate fair and insightful reviews from Andrey Grachev and two anonymous reviewers; these helped us improve our story. The U.S. National Science Foundation supported Andreas and Jordan in this work with award 10–19322. The U.S. Office of Naval Research supported Andreas with award N00014-12-C-0290 and Andreas, Mahrt, and Vickers with award N00014-11-1-0073.

References

Anderson, K., et al. (2004), The RED Experiment: An assessment of boundary layer effects in a trade winds regime on microwave and infrared propagation over the sea, *Bull. Am. Meteorol. Soc.*, *85*, 1355–1365.

Andreas, E. L (1988), Estimating C_n^2 over snow and sea ice from meteorological data, *J. Opt. Soc. Am. A Opt. Image Sci.*, *5*, 481–495.

Andreas, E. L (1989), Comments on ''A physical bound on the Bowen ratio'', *J. Appl. Meteorol.*, *28*, 1252–1254.

Andreas, E. L (1992), Uncertainty in a path-averaged measurement of the friction velocity u_*, *J. Appl. Meteorol.*, *31*, 1312–1321.

Andreas, E. L (2005), Handbook of Physical Constants and Functions for Use in Atmospheric Boundary Layer Studies, ERDC/CRREL Monogr. M-05-1, 42 pp., U.S. Army Cold Reg. Res. and Eng. Lab., Hanover, N. H.

Andreas, E. L (2010), Spray-mediated enthalpy flux to the atmosphere and salt flux to the ocean in high winds, *J. Phys. Oceanogr.*, *40*, 608–619.

Andreas, E. L (2011), Fallacies of the enthalpy transfer coefficient over the ocean in high winds, *J. Atmos. Sci.*, *68*, 1435–1445.

Andreas, E. L, and B. A. Cash (1996), A new formulation for the Bowen ratio over saturated surfaces, *J. Appl. Meteorol.*, *35*, 1281–1289.

Andreas, E. L, and J. DeCosmo (2002), The signature of sea spray in the HEXOS turbulent heat flux data, *Boundary Layer Meteorol.*, *103*, 303–333.

Andreas, E. L, and R. E. Jordan (2011), The Bowen ratio over sea ice, in 11th Conference on Polar Meteorology and Oceanography, 9 pp., Am. Meteorol. Soc., Boston, Mass., paper 1.2 (extended abstract), 2–5 May.

Andreas, E. L, R. J. Hill, J. R. Gosz, D. I. Moore, W. D. Otto, and A. D. Sarma (1998), Statistics of surface-layer turbulence over terrain with metre-scale heterogeneity, *Boundary Layer Meteorol.*, *86*, 379–408.

Andreas, E. L, P. S. Guest, P. O. G. Persson, C. W. Fairall, T. W. Horst, R. E. Moritz, and S. R. Semmer (2002), Near-surface water vapor over polar sea ice is always near ice saturation, *J. Geophys. Res.*, *107*(C10), 8033, doi:10.1029/2000JC000411.

Andreas, E. L, R. E. Jordan, and A. P. Makshtas (2004), Simulations of snow, ice, and near-surface atmospheric processes on Ice Station Weddell, *J. Hydrometeorol.*, *5*, 611–624.

Andreas, E. L, R. E. Jordan, and A. P. Makshtas (2005), Parameterizing turbulent exchange over sea ice: The Ice Station Weddell results, *Boundary Layer Meteorol.*, *114*, 439–460.

Andreas, E. L, P. O. G. Persson, and J. E. Hare (2008), A bulk turbulent air-sea flux algorithm for high-wind, spray conditions, *J. Phys. Oceanogr.*, *38*, 1581–1596.

Andreas, E. L, T. W. Horst, A. A. Grachev, P. O. G. Persson, C. W. Fairall, P. S. Guest, and R. E. Jordan (2010a), Parametrizing turbulent exchange over summer sea ice and the marginal ice zone, *Q. J. R. Meteorol. Soc.*, *136*, 927–943.

Andreas, E. L, P. O. G. Persson, R. E. Jordan, T. W. Horst, P. S. Guest, A. A. Grachev, and C. W. Fairall (2010b), Parameterizing turbulent exchange over sea ice in winter, *J. Hydrometeorol.*, *11*, 87–104.

Andreas, E. L, L. Mahrt, and D. Vickers (2012), A new drag relation for aerodynamically rough flow over the ocean, *J. Atmos. Sci.*, *69*, 2520–2537.

Arya, S. P. (1988), *Introduction to Micrometeorology*, 307 pp., Academic, San Diego, Calif.

Bentamy, A., K. B. Katsaros, A. M. Mestas-Nuñez, W. M. Drennan, E. B. Forde, and H. Roquet (2003), Satellite estimates of wind speed and latent heat flux over the global ocean, *J. Clim.*, *16*, 637–656.

Brutsaert, W. H. (1982), *Evaporation into the Atmosphere: Theory, History, and Applications*, 299 pp., D. Reidel, Dordrecht, Netherlands.

Buck, A. L. (1981), New equations for computing vapor pressure and enhancement factor, *J. Appl. Meteorol.*, *20*, 1527–1532.

Busch, N. E. (1973), On the mechanics of turbulence, in *Workshop on Micrometeorology*, edited by D. A. Haugen, pp. 1–65, Am. Meteorol. Soc., Boston, Mass.

Cronin, M. F., C. W. Fairall, and M. J. McPhaden (2006), An assessment of buoy-derived and numerical weather prediction surface heat fluxes in the Tropical Pacific, *J. Geophys. Res.*, *111*, C06038, doi:10.1029/2005JC003324.

De Bruin, H. A. R., and J. Q. Keijman (1979), The Priestley-Taylor evaporation model applied to a large, shallow lake in the Netherlands, *J. Appl. Meteorol.*, *18*, 898–903.

DeCosmo, J. (1991), Air-sea exchange of momentum, heat and water vapor over whitecap sea states, PhD thesis, 212 pp., Dep. of Atmos. Sci., Univ. of Washington, Seattle.

DeCosmo, J., K. B. Katsaros, S. D. Smith, R. J. Anderson, W. A. Oost, K. Bumke, and H. Chadwick (1996), Air-sea exchange of water vapor and sensible heat: The Humidity Exchange over the Sea (HEXOS) results, *J. Geophys. Res.*, *101*, 12,001–12,016.

Drexler, J. Z., R. L. Snyder, D. Spano, and K. T. Paw U (2004), A review of models and micrometeorological methods used to estimate wetland evapotranspiration, *Hydrol. Processes*, *18*, 2071–2101.

Dyer, A. J. (1974), A review of flux-profile relationships, *Boundary Layer Meteorol.*, *7*, 363–372.
Edson, J., et al. (2007), The Coupled Boundary Layers and Air–Sea Transfer experiment in low winds, *Bull. Am. Meteorol. Soc*., *88*, 341–356.
Eichinger, W. E., M. B. Parlange, and H. Stricker (1996), On the concept of equilibrium evaporation and the value of the Priestley-Taylor coefficient, *Water Resour. Res.*, *32*, 161–164.
Fairall, C. W., E. F. Bradley, D. P. Rogers, J. B. Edson, and G. S. Young (1996), Bulk parameterization of air-sea fluxes for Tropical Ocean-Global Atmosphere Coupled-Ocean Atmosphere Response Experiment, *J. Geophys. Res*., *101*, 3747–3764.
Fairall, C. W., E. F. Bradley, J. E. Hare, A. A. Grachev, and J. B. Edson (2003), Bulk parameterization of air-sea fluxes: Updates and verification for the COARE algorithm, *J. Clim.*, *16*, 571–591.
Finkelstein, P. L., and P. F. Sims (2001), Sampling error in eddy correlation flux measurements, *J. Geophys. Res.*, *106*, 3503–3509.
Fleagle, R. G., and J. A. Businger (1980), *An Introduction to Atmospheric Physics*, 2nd ed., 432 pp., Academic, New York.
Foken, T. (2008), The energy balance closure problem: An overview, *Ecol. Appl.*, *18*, 1351–1367.
Fuehrer, P. L., and C. A Friehe (2002), Flux corrections revisited, *Boundary Layer Meteorol.*, *102*, 415–457.
Garratt, J. R. (1992), *The Atmospheric Boundary Layer*, 316 pp., Cambridge Univ. Press, Cambridge, U. K.
Grachev, A. A., C. W. Fairall, P. O. G. Persson, E. L Andreas, and P. S. Guest (2005), Stable boundary-layer scaling regimes: The SHEBA data, *Boundary Layer Meteorol.*, *116*, 201–235.
Green, A. E., M. S. Astill, M. J. McAneney, and J. P. Nieveen (2001), Path-averaged surface fluxes from infrared and microwave scintillometers, *Agric. For. Meteorol.*, *109*, 233–247.
Guo, X., H. Zhang, L. Kang, J. Du, W. Li, and Y. Zhu (2007), Quality control and flux gap filling strategy for Bowen ratio method: Revisiting the Priestley-Taylor evaporation model, *Environ. Fluid Mech.*, *7*, 421–437.
Hicks, B. B., and G. D. Hess (1977), On the Bowen ratio and surface temperature at sea, *J. Phys. Oceanogr.*, *7*, 141–145.
Högström, U. (1996), Review of some basic characteristics of the atmospheric surface layer, *Boundary Layer Meteorol.*, *78*, 215–246.
Hsu, S. A. (1998), A relationship between the Bowen ratio and sea-air temperature difference under unstable conditions at sea, *J. Phys. Oceanogr.*, *28*, 2222–2226.
Jackson, D. L., and G. A. Wick (2010), Near-surface air temperature retrieval derived from AMSU-A and sea surface temperature observations, *J. Atmos. Oceanic Technol.*, *27*, 1769–1776.
Jo, Y.-H., X.-H. Yan, J. Pan, M.-X. He, and W. T. Liu (2002), Calculation of the Bowen ratio in the tropical Pacific using sea surface temperature data, *J. Geophys. Res.*, *107*(C9), 3134, doi:10.1029/2001JC001150.
Kaimal, J. C., and J. E. Gaynor (1991), Another look at sonic thermometry, *Boundary Layer Meteorol.*, *56*, 401–410.
Kim, C. P., and D. Entekhabi (1997), Examination of two methods for estimating regional evaporation using a coupled mixed layer and land surface model, *Water Resour. Res.*, *33*, 2109–2116.
Konda, M., N. Imasato, and A. Shirata (1996), A new method to determine near-sea surface air temperature by using satellite data, *J. Geophys. Res.*, *101*, 14,349–14,360.
Kunkel, K. E., and D. L. Walters (1983), Modeling the diurnal dependence of the optical refractive index structure parameter, *J. Geophys. Res.*, *88*, 10,999–11,004.
Lewis, J. M. (1995), The story behind the Bowen ratio, *Bull. Am. Meteorol. Soc.*, *76*, 2433–2443.
Lhomme, J.-P. (1997), A theoretical basis for the Priestley-Taylor coefficient, *Boundary Layer Meteorol.*, *82*, 179–191.
Liu, W. T. (1986), Statistical relation between monthly mean precipitable water and surface-level humidity over global ocean, *Mon. Weather Rev.*, *114*, 1591–1602.
Liu, W. T. (1988), Moisture and latent heat flux variabilities in the tropical Pacific derived from satellite data, *J. Geophys. Res.*, *93*, 6749–6760.
Mahrt, L., and D. Khelif (2010), Heat fluxes over weak SST heterogeneity, *J. Geophys. Res.*, *115*, D11103, doi:10.1029/2009JD013161.
Mahrt, L., J. Sun, W. Blumen, T. Delany, and S. Oncley (1998), Nocturnal boundary-layer regimes, *Boundary Layer Meteorol.*, *88*, 255–278.
Mahrt, L., D. Vickers, E. L Andreas, and D. Khelif (2012), Sensible heat flux in near-neutral conditions over the sea, *J. Phys. Oceanogr.*, *42*, 1134–1142.
McNaughton, K. G. (1976), Evaporation and advection: I. Evaporation from extensive homogeneous surfaces, *Q. J. R. Meteorol. Soc.*, *102*, 181–191.
Oncley, S. P., et al. (2007), The Energy Balance Experiment EBEX-2000. Part I: Overview and energy balance, *Boundary Layer Meteorol.*, *123*, 1–28.
Panofsky, H. A., and J. A. Dutton (1984), *Atmospheric Turbulence: Models and Methods for Engineering Applications*, 397 pp., John Wiley, New York.
Persson, P. O. G. (2012), Onset and end of the summer melt season over sea ice: Thermal structure and surface energy perspective from SHEBA, *Clim. Dyn.*, *39*, 1349–1371.
Persson, P. O. G., C. W. Fairall, E. L Andreas, P. S. Guest, and D. K. Perovich (2002), Measurements near the Atmospheric Surface Flux Group tower at SHEBA: Near-surface conditions and surface energy budget, *J. Geophys. Res.*, *107*(C10), 8045, doi:10.1029/2000JC000705.
Persson, P. O. G., J. E. Hare, C. W. Fairall, and W. D. Otto (2005), Air-sea interaction processes in warm and cold sectors of extratropical cyclonic storms observed during FASTEX, *Q. J. R. Meteorol. Soc.*, *131*, 877–912.
Petersen, G. N., and I. A. Renfrew (2009), Aircraft-based observations of air-sea fluxes over Denmark Strait and the Irminger Sea during high wind speed conditions, *Q. J. R. Meteorol. Soc.*, *135*, 2030–2045.
Philip, J. R. (1987), A physical bound on the Bowen ratio, *J. Clim. Appl. Meteorol.*, *26*, 1043–1045.
Philip, J. R. (1989), Reply, *J. Appl. Meteorol.*, *28*, 1255.
Priestley, C. H. B., and R. J. Taylor (1972), On the assessment of surface heat flux and evaporation using large-scale parameters, *Mon. Weather Rev.*, *100*, 81–92.
Raupach, M. R. (2001), Combination theory and equilibrium evaporation, *Q. J. R. Meteorol. Soc.*, *127*, 1149–1181.
Romero, L., and W. K. Melville (2010), Airborne observations of fetch-limited waves in the Gulf of Tehuantepec, *J. Phys. Oceanogr.*, *40*, 441–465.
Saunders, P. M. (1964), Sea smoke and steam fog, *Q. J. R. Meteorol. Soc.*, *90*, 156–165.
Schotanus, P., F. T. M. Nieuwstadt, and H. A. R. De Bruin (1983), Temperature measurement with a sonic anemometer and its application to heat and moisture fluxes, *Boundary Layer Meteorol.*, *26*, 81–93.
Schulz, J., P. Schlüssel, and H. Grassl (1993), Water vapor in the atmospheric boundary layer over oceans from SSM/I measurements, *Int. J. Remote Sens.*, *14*, 2773–2789.
Stull, R. B. (1988), *An Introduction to Boundary Layer Meteorology*, 666 pp., Kluwer, Dordrecht, Netherlands.
Sun, J., J. F. Howell, S. K. Esbensen, L. Mahrt, C. M. Greb, R. Grossman, and M. A. LeMone (1996), Scale dependence of air-sea fluxes over the Western Equatorial Pacific, *J. Atmos. Sci.*, *53*, 2997–3012.
Sun, J., D. Vandemark, L. Mahrt, D. Vickers, T. Crawford, and C. Vogel (2001), Momentum transfer over the coastal zone, *J. Geophys. Res.*, *106*, 12,437–12,488.
Thadathil, P., Y. Sugimori, and M. Akiyama (1995), Surface heat fluxes using satellite observations: A case study in the northwest Pacific, *J. Atmos. Oceanic Technol.*, *12*, 1071–1086.
Uttal, T., et al. (2002), Surface Heat Budget of the Arctic Ocean, *Bull. Am. Meteorol. Soc.*, *83*, 255–275.
Vickers, D., and S. K. Esbensen (1998), Subgrid surface fluxes in fair weather conditions during TOGA COARE: Observational estimates and parameterization, *Mon. Weather Rev.*, *126*, 620–633.
Vickers, D., L. Mahrt, and E. L Andreas (2013), Estimates of the 10-m neutral sea surface drag coefficient from aircraft eddy-covariance measurements, *J. Phys. Oceanogr.*, *43*, 301–310.
Webb, E. K., G. I. Pearman, and R. Leuning (1980), Correction of flux measurements for density effects due to heat and water vapour transfer, *Q. J. R. Meteorol. Soc.*, *106*, 85–100.
Wesley, M. L. (1976), The combined effect of temperature and humidity fluctuations on refractive index, *J. Appl. Meteorol.*, *15*, 43–49.
Wyngaard, J. C. (2010), *Turbulence in the Atmosphere*, 393 pp., Cambridge Univ. Press, Cambridge, U. K.